

## Article

# The Influence of Pore Distribution of Coal Char in the Char Fragmentation and Included Minerals Partitioning: A Percolation Modeling

Rui Li <sup>1,2</sup>, Zhenqi Jing <sup>2</sup>, Jingjing Ma <sup>3</sup>, Long Qin <sup>2</sup>, Kai Yan <sup>1,2</sup> and Chang Wen <sup>1,2,\*</sup>

<sup>1</sup> China-EU Institute for Clean and Renewable Energy, Huazhong University of Science and Technology, Wuhan 430074, China; rayleapan@hust.edu.cn (R.L.); iyankai@hust.edu.cn (K.Y.)

<sup>2</sup> Department of New Energy Science and Engineering, School of Energy and Power Engineering, Huazhong University of Science and Technology, Wuhan 430074, China; m202071232@hust.edu.cn (Z.J.); u201911506@hust.edu.cn (L.Q.)

<sup>3</sup> State Key Laboratory of High-efficiency Utilization of Coal and Green Chemical Engineering, Ningxia University, Yinchuan 750021, China; majingjing@nxu.edu.cn

\* Correspondence: wenchang@hust.edu.cn; Tel.: +86-27-87544779

**Abstract:** The processes of char fragmentation, including mineral partitioning and particulate matter (PM) formation during dense and porous char combustion, were observed by a site percolation model. This model simulated the diffusion-controlled regime of char combustion, and the size distributions of included minerals in typical bituminous coal were determined by the computer-controlled scanning electron microscope (CCSEM), and the data were put into the char matrix randomly. The model presents the influence of initial pore distribution on char oxidation and fragmentation, the impact of the char conversion process on the extent of fragmentation, the change of ash distributions with the char conversion, and the particulate matters (PM) size distribution, which is derived from the consequence of the competition between char fragmentation and included minerals partitioning and coalescence. The results indicate that with increasing initial char porosity ( $\phi$ ), the number of large size pores increases but the number of pores decreases, which leads to open pores increasing, close pores decreasing, and the surface reaction area increasing. While  $\phi \geq 0.4$ , char fragmentation obviously occurs during the stage in which the rates of char conversion are 0.4–0.6, and it looks as though the maximum value of fragmentation will transfer to an earlier conversion stage if it has a larger  $\phi$ . The enhanced  $\phi$  shows a positive effect on the increase in the number and concentration of PM < 10  $\mu\text{m}$  (nominally aerodynamic diameter), this is attributed to char fragments more drastically, and the probability of mineral coalescence reduces a lot.

**Keywords:** percolation model; char fragmentation; mineral partitioning; CCSEM; particulate matter



**Citation:** Li, R.; Jing, Z.; Ma, J.; Qin, L.; Yan, K.; Wen, C. The Influence of Pore Distribution of Coal Char in the Char Fragmentation and Included Minerals Partitioning: A Percolation Modeling. *Atmosphere* **2022**, *13*, 628. <https://doi.org/10.3390/atmos13040628>

Academic Editor:  
Jaroslaw Krzywanski

Received: 21 March 2022

Accepted: 11 April 2022

Published: 15 April 2022

**Publisher's Note:** MDPI stays neutral with regard to jurisdictional claims in published maps and institutional affiliations.



**Copyright:** © 2022 by the authors. Licensee MDPI, Basel, Switzerland. This article is an open access article distributed under the terms and conditions of the Creative Commons Attribution (CC BY) license (<https://creativecommons.org/licenses/by/4.0/>).

## 1. Introduction

Coal-fired power plants bring adverse environmental and health impacts, such as SO<sub>x</sub>, NO<sub>x</sub>, mercury, and particulate matter [1–3]. Particulate matter with an aerodynamic diameter of fewer than 10  $\mu\text{m}$  is seriously harmful to human health, which cannot be efficiently precipitated by conventional air pollution control devices [4]. Therefore, part of them will be inevitably emitted into the atmosphere, causing air pollution, and increasing the risk of asthma attacks, cardiopulmonary problems, lung cancer, and other diseases. Classical studies attempted to describe fly ash formation during pulverized coal combustion as a bimodal particle size distribution (PSD) produced by two dominant mechanisms [5,6]: fragmentation and included minerals coalescence (super-micron mode, >1  $\mu\text{m}$ ) and vaporization/nucleation (ultrafine mode, 0.1–1  $\mu\text{m}$ ). In recent years, some studies [7–10] revealed that pulverized coal fly ash particle formation is more accurately described as a tri-modal PSD that includes a central mode (fine fragmentation mode, approximately

2–5  $\mu\text{m}$ ). Although the formation mechanism of the central mode is not well understood now, we know it still mainly comes from char fragmentation.

Char fragmentation may play a significant role in pulverized coal combustion [11,12], and it may not change fine pores per unit volume but may change open porosity and external surface area, causing the rates of char conversion to increase and the rates of unburnt carbon to decrease [13–15]. Furthermore, char fragmentation is important to particulate matters formation; the increase in particle number and the decrease in particle size were found as the char burnout rate enhanced [8,16–18]. Char fragmentation is affected by synergic effects of some factors, and some research results indicated pore structure of char was the decisive factor in char fragmentation. A number of researchers [16,19,20] studied the fragmentation behavior of some carbonaceous substances under various oxidation regimes. They suggested char fragmentation has been found to be associated with the porous structure of char particles, especially the macropores ( $>0.05 \mu\text{m}$ ), which provide channels for transporting oxidizing gas from the external environment to the internal surface and have been shown to play a significant role in char fragmentation during diffusion-controlled reactions. Helble et al. [10] presented reaction gas could penetrate the interior of a particle so that an oxidation reaction could progress in both the inner and outer surface of the particle simultaneously, which caused the combustion reaction more drastically and fragmentation more frequently, at last, it may form a number of smaller ash particles (mainly  $\text{PM}_{1.0+}$ ) if oxidation causes the carbon bonds of char particle to break up. Liu et al. [21] pointed out that the reduction of pulverized coal particle size would increase the proportion of extrinsic minerals, leading to more extrinsic minerals being directly converted to  $\text{PM}_{10}$ . At the same time, smaller particle size will also lead to an increase in combustion temperature, resulting in more distance of mineral fragmentation and an increase in the amount of  $\text{PM}_1$ . In addition, as the carbonaceous surface recedes during combustion, the imbedded minerals (included minerals) are exposed to the surface gradually, and a number of surface minerals melt and turn into spherical ash droplets and the distance of ash droplets grows closer and closer. As a consequence, they may partition and coalesce into ash particles (mainly  $\text{PM}_{1.0+}$ ) while they contact each other, and a part of the mineral grains may shed off as well. The process of  $\text{PM}_{1.0+}$  formation, therefore, is governed by the competition between the fragmentation of char particles and the coalescence of included mineral particles on the char surface. Char fragmentation influences both the particulate matter size distribution and the final particle number—the more the extent of char fragmentation is, the less mineral coalescence occurs, which generates a greater number of particles and causes particles to become smaller. Up to now, the process of change in pore structure and mineral size during char fragmentation cannot be clarified through experimental methods.

Computer simulation has been used as an alternative to the experimental study to describe the pore structure evolution in coal char, the fragmentation behavior of char, and the particulate matter formation. Percolation fragmentation refers to the transition from a connected, solid network to a completely fragmented state; the process of char fragmentation is proven to be a percolation behavior. Percolation theory [16,18,22–24] has already been applied to char combustion and fragmentation extensively. Kang et al. [22] and Helble et al. [16] performed the simulation of char oxidation and fragmentation based on a percolation model on a lattice and studied the char fragmentation and residual ash formation. Yu et al. [23,24] set up a two-dimension fragmentation model of a single char particle based on a site percolation model during an external diffusion-controlled regime; they predicted that the relation between initial porosity and the extent of fragmentation, the impact of pore structure, and the extent of fragmentation on residual ash sizes, whereas, they supposed the mineral size is a fixed value, which is rather different from the actual size distribution of minerals in coal.

The objective of this paper is to simulate the process of char combustion and mineral conversion and obtain the particle number and concentration distribution, especially particles of 1–10  $\mu\text{m}$ . We optimize the site percolation model and choose the included mineral size measured by CCSEM as the initial mineral data used in this model so that

it can ensure a result that is close to the actual size distribution of included minerals in coal [25].

## 2. Model Formulation

### 2.1. Model Hypothesis

During the devolatilization stage, different types of char structures are generated according to the difference of organic character and char thickness [26], namely cenospheric char ( $\varphi > 65\%$ ), porous char ( $\varphi = 40\text{--}65\%$ ), and dense char ( $\varphi < 40\%$ ).

1. The char fragmentation is neglected, and the char swelling ratio is supposed to be finite during coal pyrolysis, therefore generating little cenospheric char. The largest initial porosity in the reaction is 0.5. Therefore, the char conversion is reviewed in the range of  $\varphi = 10\text{--}50\%$ , which belongs to dense char and porous char.
2. Only considering the influence of macropores ( $>0.05\ \mu\text{m}$ ) during char combustion in the external diffusion-controlled regime, and the char oxidation reaction could proceed inside and outside the particle simultaneously.
3. It is assumed that all the minerals exist in the form of fine spherical particles, and their densities are constants, neglecting the influence of excluded minerals in the model because it can be removed through a physical method. Wang et al. [27] made a similar assumption in their model.
4. During char combustion, minerals do not vaporize, crash and take place chemical reaction; two particles gather their volumes as they contact each other and find a new size supposing the new particle is still a sphere. Generally, the mass of inorganic mineral vaporization is less than 5% of total mineral mass [28], so it would not have a significant effect on the final size distribution of  $\text{PM}_{1-10}$ .
5. No hollow ash particles are formed. The aggregate volume of the two minerals is the sum of the previous two, and the mass of the new particulate is the sum of the previous two.

### 2.2. Initial Model

This model permits variation of the parameters shown to be important experimentally—porosity, mineral matter inclusion size, and mineral loading. Our site percolation model of char fragmentation and included mineral partitioning represents a char particle as a cluster of connected occupied sites randomly distributed on a two-dimensional square lattice. It has been previously indicated that the particle size obtained by the 2D simulation is close to that obtained from a 3D calculation [19–22];  $N \times N$  square-shaped cluster is generated on a matrix of a given size. In the cluster, two contiguous sites, which are represented by '1', are defined as being connected, with all occupied sites containing an equal fraction of the carbon mass of the initial char particle.

The macropores distribute in the shell randomly so as to approximately match the measured porosity ' $\varphi$ ' and surface area are represented by unoccupied sites and '0', and the ambient external to the cluster is defined to be the reactant gas. The carbon and pore are brown and white pixels, respectively, in Figure 1. In the matrix, if the initial porosity is  $\varphi$ , the number of occupied sites is  $N^2(1 - \varphi)$ , and that of unoccupied sites is  $N^2\varphi$ . Those pores are directly exposed to ambient conditions, allowing oxygen to penetrate the pores. The reaction is possible only when a given char site is directly in contact with an oxidizing environment implying kinetic controlled combustion. Minerals considered as a uniform sphere in all cases are distributed among every given char site as an initial condition. At the start of the program, there exists a char matrix constituted by occupied sites '1' and unoccupied sites '0' to control the process of char combustion, and another mineral matrix that all occupied sites '1' is replaced by mineral size, which is decided by CCSEM in random to control the process of particulate matters formation.

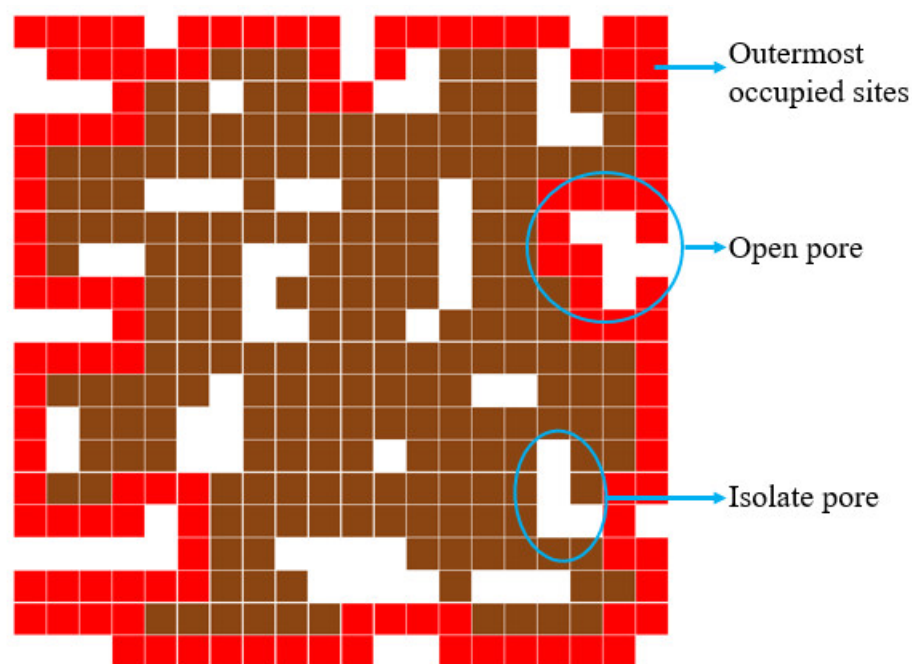


**Figure 1.** Char matrix and outermost occupied sites.

It can be assumed that pore distributes randomly in char particle; thus, there exists both an open pore which connects with the ambient and an isolate pore (that is, close pore) that reactant gas cannot enter into in the initial char matrix. The initial random distribution must ensure that all occupied sites connect to each other; in other words, any fragments formed during the generation of the matrix are removed. Oxidation and combustion of the particle are represented by random removal of sites from the perimeter of the cluster, with the perimeter determined by checking the connectivity of pores to the ambient. Char bonds in contact with the ambience burn at a mean rate that depends on cluster size. No interior sites are removed until the outermost sites (all occupied sites connecting the ambient) have been completely removed, thereby simulating reaction in the external diffusion-controlled regime. The outermost site is drawn as red in Figure 1. The occupied site would turn to the pore after it is oxidized in the char matrix, and the mineral matter in the char matrix that was associated with the reacted site is redistributed to one of the nearest-neighboring char sites randomly. The ash mass of the chosen neighboring site is therefore increased by the amount of ash associated with the just reacted site, and the ash content of the reacted site is redefined as zero. Once there is no occupied site around the ash particles, they are separated from the whole char model, then fragmented ash particle is formed. All the changes in the ash content of the sites are recorded. Fragmentation is modeled as the separation of occupied sites into disconnected pieces due to bond burnout. The judgement of connectivity about mineral transformation and fragmentation adopts the 8-connection rule, which means a site connects its eight surrounding lattices. The process of reaction, char fragmentation, and ash coalescence continue until all of the char sites have been removed. The number of removed carbon sites during each layer represents the relative reaction rate.

### 2.3. The Input of Initial Mineral Size

The initial mineral distribution in char is determined by CCSEM (Computer Controlled Scanning Electron Microscopy, Quanta 200 FEI, Hillsboro, OR, USA). CCSEM is a one-by-one analytical technology; it can analyse a large number of mineral particles individually, commonly more than 3000 particles, and obtain the physical parameter of every particle, such as elements, sizes, and shape. At last, the information about every mineral is obtained through a specific analysis [26,29]. Comparing the technology of Laser Particle Sizer and

SEM-EDS, the advantage of CCSEM is that it can quantitatively determine the distribution of specific mineral sizes and distinguish included minerals. Thus, it can represent the initial mineral distribution in the simulated char particles.

Most of the included minerals measured by CCSEM are 1–50  $\mu\text{m}$ , and the smallest particle size that can be measured is about 0.5  $\mu\text{m}$ . More details about CCSEM can be found in other papers [30,31].

The initial mineral matrix is accomplished according to the following steps:

1. Measuring more than 4000 particles by CCSEM, an  $N \times N$  matrix is constituted by these data, then the order of all data will be changed through a program of “random” accompanied by Matlab (MATLAB 2017a, The MathWorks, Inc., Natick, MA, USA) software. Table 1 shows the number and detailed size distribution of included minerals measured by CCSEM.
2. We should find all pore sites in the char matrix and let the data of these sites in the mineral matrix be ‘0’ to ensure that the porosities of these two matrices are identical.

**Table 1.** Initial mineral distribution in char measured by CCSEM.

<b>Geometrical Diameter D (<math>\mu\text{m}</math>)</b>	<b>0.5–1</b>	<b>1–2</b>	<b>2–3</b>	<b>3–4</b>	<b>4–5</b>
Number	504	1464	2096	230	223
<b>Geometrical Diameter D (<math>\mu\text{m}</math>)</b>	<b>5–6</b>	<b>6–7</b>	<b>7–8</b>	<b>8–9</b>	<b>9–10</b>
Number	167	58	53	32	28

#### 2.4. The Program of Char Conversion and Mineral Partitioning

1. Firstly, we need to obtain surface occupied sites from the char matrix, then choose an occupied site  $O_i$  which has a mineral volume of  $V_i$  as the first reactive site.
2. According to the 8-connection rule, if  $O_i$  has adjacent occupied sites, one of these, such as  $O_k$  with volume a of  $V_k$ , will be chosen to obtain the mineral from  $O_i$ , then mineral in  $O_i$  is 0, and the site  $O_i$  in char matrix is 0. The mineral volume of site  $O_k$  becomes  $V_i + V_k$  now.
3. If  $O_i$  has no adjacent occupied sites, the mineral in site  $O_i$  will be regarded as ash which no longer connects with other minerals and is stored in the mineral matrix, then the mineral in  $O_i$  is 0, and the site  $O_i$  in the char matrix is 0, too.
4. Repeat steps 1–3 until the reaction of the surface occupied sites of this layer is complete.
5. Carrying out the reaction of the next layer through continuing steps 1–4, the program finishes as the reaction of all layers is complete. At last, it is all ‘0’ in the char matrix, the final mineral matrix is the ash matrix, and the data should be transferred from ash minerals volume to these sizes. The procedure is described in Figure 2.

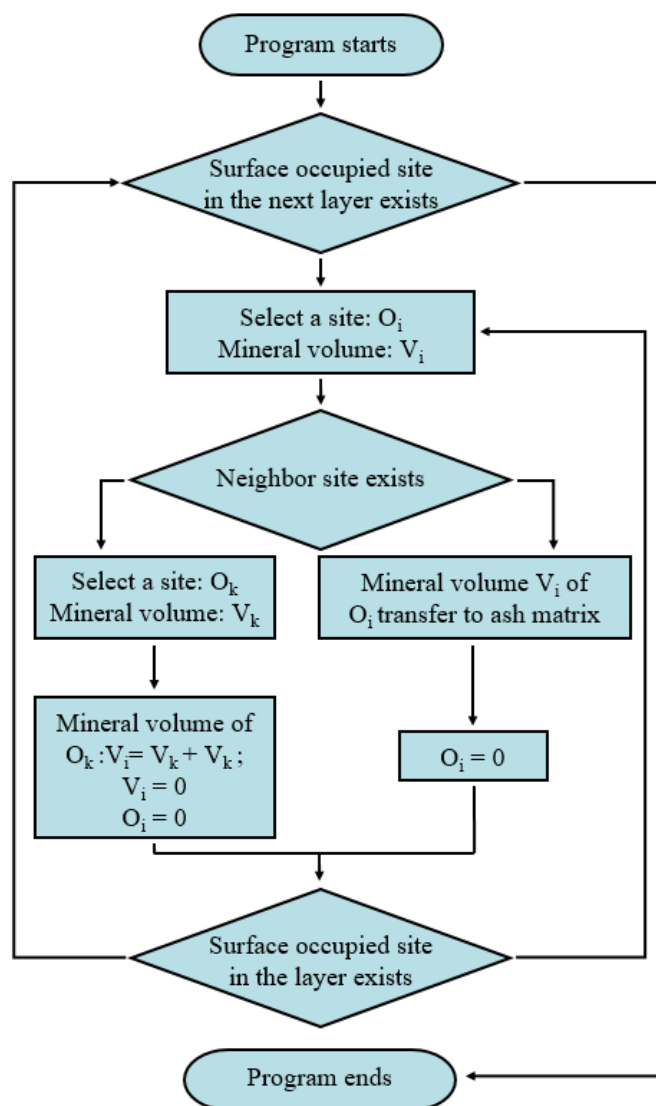


Figure 2. Procedure of program for char conversion and mineral partitioning.

### 3. Results and Discussion

#### 3.1. Initial Pore Distribution

The initial pore distribution is plotted in Figure 3. When initial porosity ( $\varphi$ ) is a low value ( $\varphi = 0.1$ ), the size of pore clusters is small, but the number is large. The pores are spread in the matrix sparsely, and most of these are isolated pores. For comparison, if having a large  $\varphi$  ( $\varphi = 0.4$ ), the number of large size pore clusters increases obviously, and many open pores can be observed. The tendency of pore structure change is drawn in Figure 4. As  $\varphi$  increases, the number of open pore clusters, isolate pore clusters, and total pore clusters first increase and then decrease. On the one hand, most of the pores are small and isolated at first, and the number of small size pores increases gradually with increasing  $\varphi$  to 0.2; on the other hand, some small pores merge into the larger pores and lead to the number of small pores decreases and that of large pores increases. As  $\varphi$  increases, the number of decreased pores is larger than that of the increased ones, leading to the total number decreases. At the same time, plenty of isolated pores are combined with open pores so that the number of isolated pores decreases since  $\varphi = 0.2$  and that of open pores decreases since  $\varphi = 0.3$ .

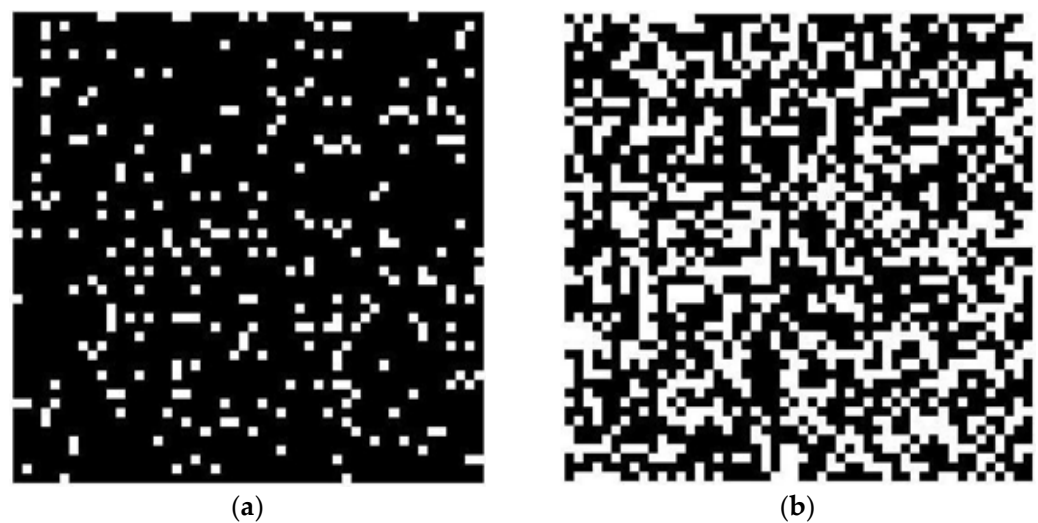


Figure 3. Initial pore distribution: (a)  $\varphi = 0.1$ ; (b)  $\varphi = 0.4$ .

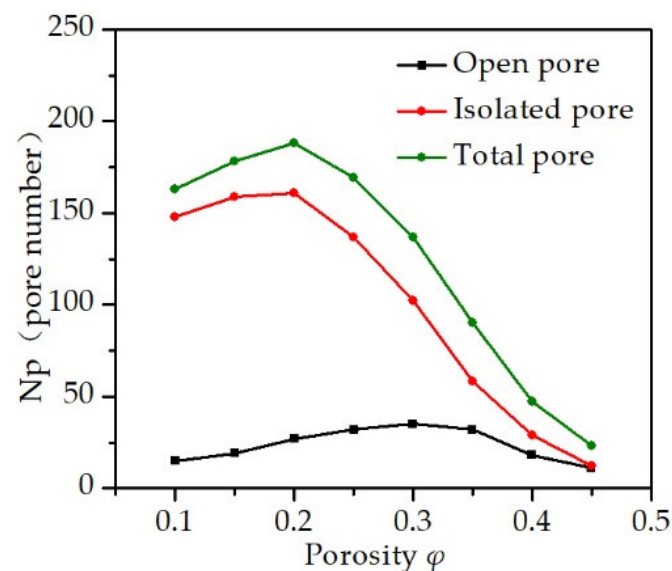
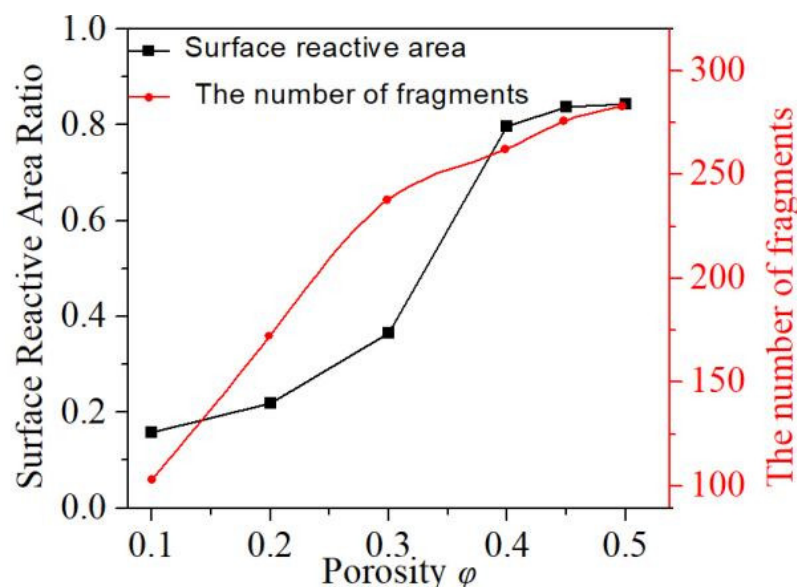


Figure 4. Pore number changing as  $\varphi$  increases.

### 3.2. Impact of Initial Porosity on Char Fragmentation

The initial number of surface occupied sites in the char matrix represents the initial surface reaction area. With the reaction area increasing, char combustion progresses more rapidly, and fragmentation occurs more frequently. As is shown in Figure 5, increasing porosity enhances the surface reaction area and the number of fragments, and the increase in reaction area leads to an increase in the number of fragments. Compared with  $\varphi < 0.4$ , the number of fragments and the surface reaction area while  $\varphi \geq 0.4$  increase obviously. These differences in the surface reaction area and the extent of fragmentation are caused in part by the different char properties [32]. The char of  $\varphi < 0.4$  is mainly dense char which has a high density. It almost does not swell, and most of this is aggregate which forms ash during char combustion. However, the char of  $\varphi \geq 0.4$  is mainly porous char, which has a non-uniform pore distribution that mostly breaks up to form fine ash.



**Figure 5.** Surface reactive area and the number of fragments.

### 3.3. Impact of Char Conversion on Char Fragmentation

Char conversion was calculated by dividing the total loss of carbon sites after each layer by the initial number of carbon sites, and the extent of fragmentation is defined as the rates of the number of fragments at every layer to the total number of fragments. Subsequently, we plot Figures 6 and 7. Figure 6a presents the relation between porosity and the rate of reaction, which is reflected by the loss of carbon sites. All the carbon sites in the char of  $\phi = 0.45$  are oxidized in the second step, while only 30% and 70% of carbon sites are lost in the char of  $\phi = 0.2$  and  $\phi = 0.3$ . The char of  $\phi \geq 0.3$  has finished the reaction before the fourth step, while the char of  $\phi = 0.2$  has only reacted 60% at this step. In Figure 6b, the good relevance can be observed between char conversion and fragmentation; while  $\phi = 0.2$ , conversion and fragmentation in every layer are relatively uniform. With  $\phi$  increases, char conversion and fragmentation focus on the first two layers, which means that increasing  $\phi$  causes reaction focuses on the early stage of combustion. As  $\phi$  is a small value, the initial pore distributes extensively, and the conversion of every layer during combustion is clearly similar, then result in the extent of fragmentation in every layer being almost the same. Nevertheless, when  $\phi$  is a larger value, the initial pore distribution is irregular, the surface reaction area increases a lot, and oxidizing reaction progresses quickly during the early stage of combustion so that the conversion and the extent of fragmentation in the early stage are drastic.

Subsequently, the procedure of char conversion is divided into five uniform stages, and the extent of fragmentation of every stage is calculated, which is plotted in Figure 7. The mode of char fragmentation varies with initial porosity. The char fragmentation concentrates in the early stage of char conversion and increases gradually with increasing initial porosity. For  $\phi \leq 0.3$ , the char fragmentation is relatively uniform at every stage and becomes more drastic in the later conversion stage, which is because the fragmentation of dense particles by perimeter percolation also occurs during the later stages of combustion where particles approach critical porosity, and for  $\phi \geq 0.4$ , char fragmentation is high on the conversion range of 0.4–0.6, and the tendency for a peak value transferring to the earlier conversion stage can be found. Liu et al. [18] studied the fragmentation of cenospheric char ( $\phi > 0.5$ ) during the combustion of Australian bituminous coal; they also found that char fragmentation was severe in the stage of 30–50%, which proves our deduction about the peak value transferring to the earlier stage as  $\phi \geq 0.4$ . In the actual combustion, the increased heating rate can accelerate the devolatilization process, and the oxidation rate of

coal coke surface, then the large pore volume increases rapidly, and the coal coke crushing is more intense, perhaps enhancing the generation of PM<sub>10</sub>.

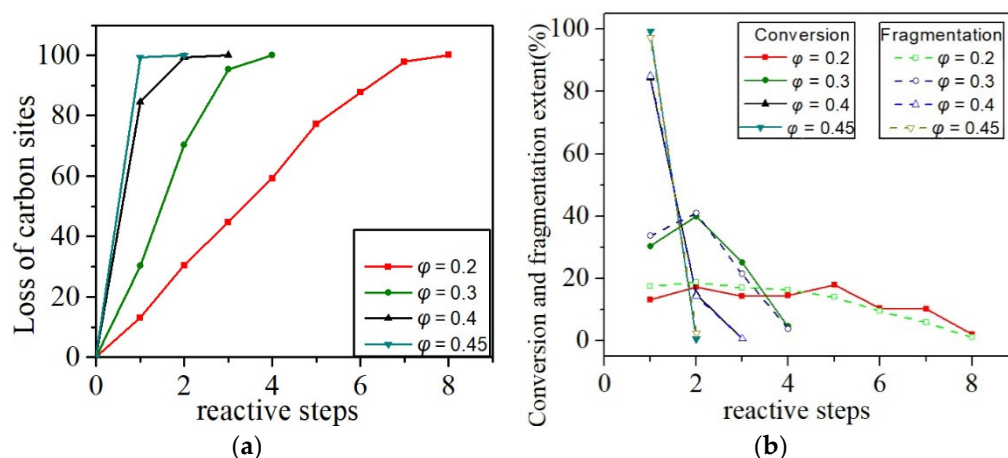


Figure 6. Char conversion: (a) The loss of carbon sites increases with reactive steps; (b) Char conversion and the extent of fragmentation.

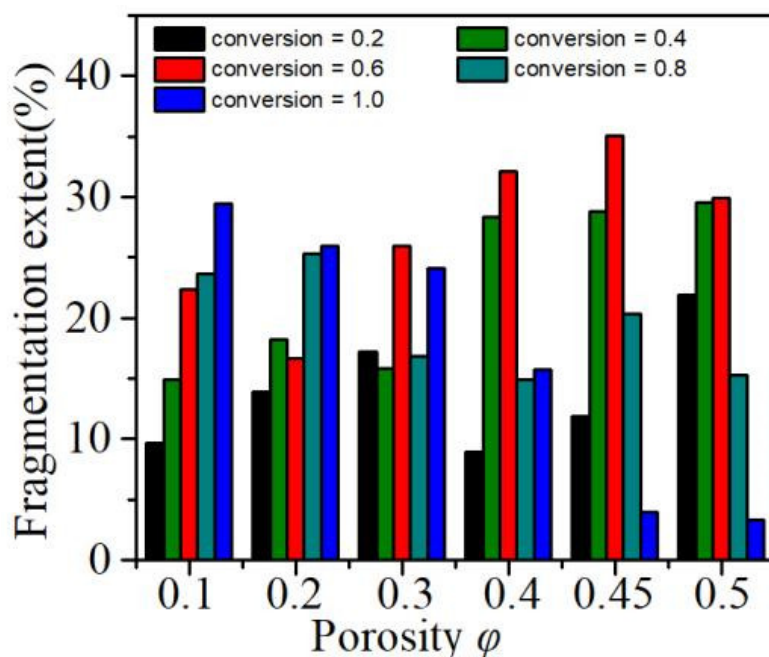
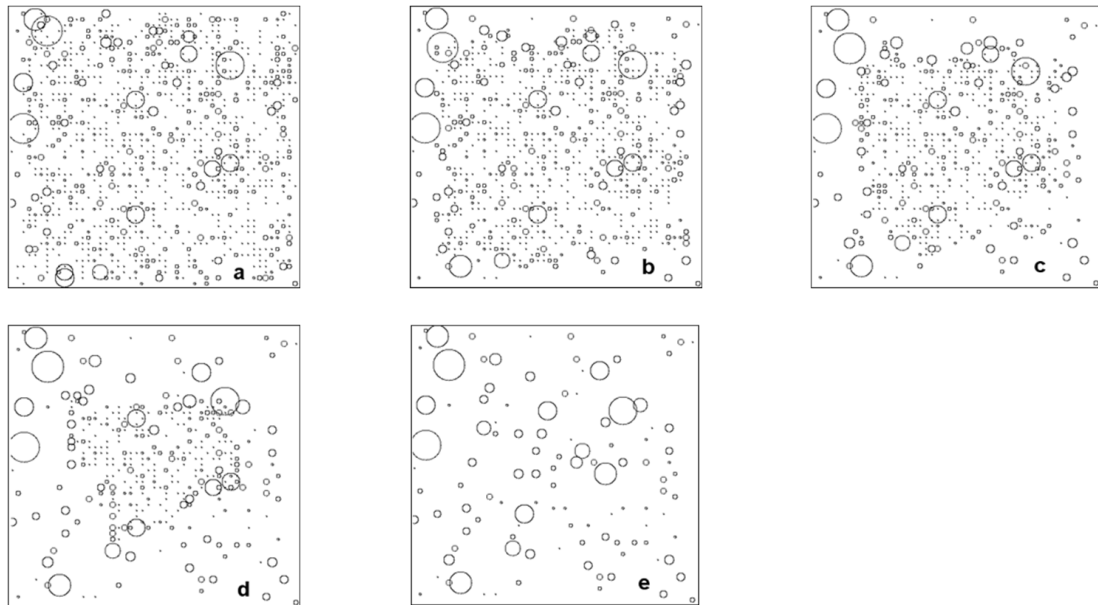


Figure 7. Change of char fragmentation with increasing char conversion.

### 3.4. The Change of Ash Distributions with the Char Conversion

The change of fine particulate matter sizes during char combustion is hardly studied through experiments. Simulating the procedure of mineral size-changing can work as a supplement and give a thorough explanation. The ash distributions from two typical porosity of  $\phi = 0.1$  and  $\phi = 0.4$  are shown in Figures 8 and 9. These figures show the ash particles  $>1 \mu\text{m}$ , and all of the ash is deemed to be spherical. When char combustion progresses, most surface minerals aggregate with the minerals exposed from the char interior, and hence, the sizes of inner minerals are eventually increased. In addition, a portion of surface minerals are left in the external layer of the char because macropore behavior causes char fragmentation; this surface ash will no longer aggregate with inner minerals and become a single ash particle. As the reaction progresses, the number of ash particles in the char matrix decreases dramatically, especially the fine particles; most of the ash aggregate forms the PM in a size range of 1–10  $\mu\text{m}$ . For  $\phi = 0.1$ , there exist

abundant fine particles distributing extensively in the beginning period of char conversion. As  $\varphi = 0.4$  has fine particles, they distribute more dispersedly in the beginning period of char conversion so that it will break up more frequently during the char conversion, that is to say, the final ash number of  $\varphi = 0.4$  is more than  $\varphi = 0.1$ . The number of 1–10  $\mu\text{m}$  PM increase for  $\varphi = 0.4$ , as does the concentration.



**Figure 8.** Procedure of mineral size transformation as  $\varphi = 0.1$ : (a) Conversion = 20.0%; (b) Conversion = 40.0%; (c) Conversion = 60.0%; (d) Conversion = 80.0%; (e) Conversion = 100%.

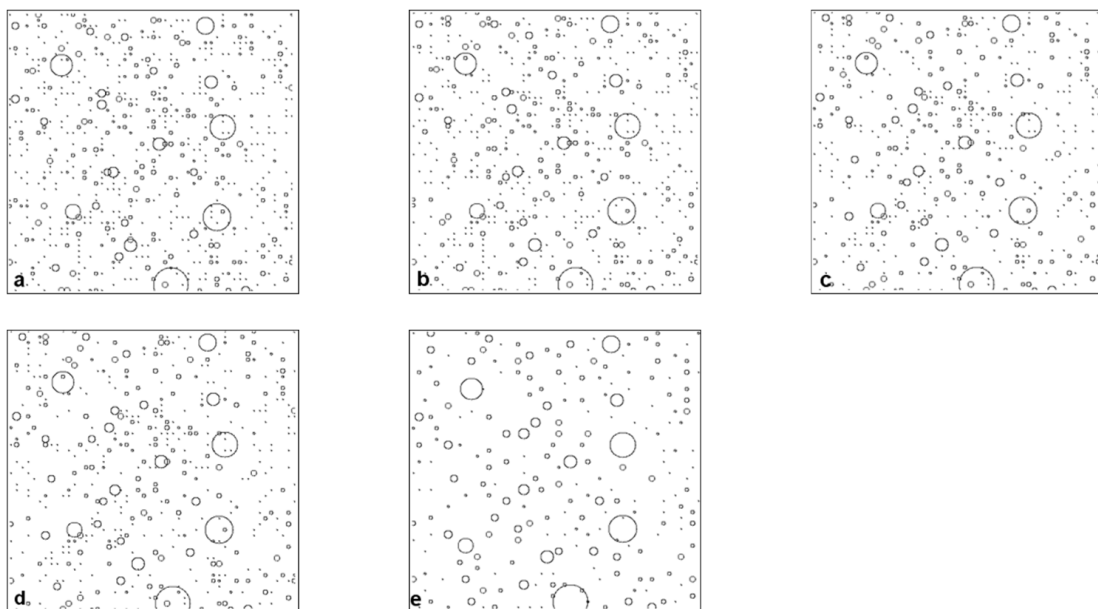


**Figure 9.** Procedure of mineral size transformation as  $\varphi = 0.4$ : (a) Conversion = 20.0%; (b) Conversion = 40.0%; (c) Conversion = 60.0%; (d) Conversion = 80.0%; (e) Conversion = 100%.

### 3.5. The Final Particle Size Distribution

The mineral and ash sizes tested by CCSEM indicate the geometrical diameter, but the particulate matters express the size by the aerodynamic diameter. Edwards et al. [33]

gave the approximate conversion formula of aerodynamic diameter  $D_p$  and geometrical diameter  $D$ :

$$D_p = D \times \sqrt{\rho} \quad (1)$$

where  $\rho$  is the density of ash particles.

The PDS bituminous coal used in this paper has low expansibility and mostly contains kaolinite, Fe aluminosilicate, and quartz. The proportion of expansion particles in ashes generated after combustion is very small [34]. Therefore, the respective densities of ash particles can be regarded as the corresponding particle density after CCSEM analysis, and the geometric particle size of ash tested by CCSEM can be converted into the aerodynamic diameter of particles. Accordingly, all data below are described in terms of aerodynamic diameter.

The final ash particles, therefore, have sizes that range from the smallest mineral inclusion size in the coal to that of a particle containing the largest portion of the initial ash content. At zero porosity, all of the ash particles remain on the char surface throughout the entire combustion process, continuing to coalesce. In this extreme case, one ash particle is generated. The ash particles below  $0.5 \mu\text{m}$  are mostly formed by a vaporization and condensation process and are not pertinent to the present discussion. The particle number size distribution from different initial porosity is drawn in Figure 10. The final number of  $\text{PM} < 10 \mu\text{m}$  is smaller than that of the original mineral, but the number of  $\text{PM} > 10 \mu\text{m}$  is relatively similar to that of the original minerals. Since a lot of included minerals aggregate during char combustion,  $\text{PM} < 10 \mu\text{m}$  decreases and forms coarse particles mainly coming from mineral coalescence. The number of  $\text{PM} < 1 \mu\text{m}$  is the most for  $\varphi = 0.5$ , but the total number is only 8% of particles  $< 1 \mu\text{m}$  of original minerals, and for  $\varphi = 0.1$ , the ratio is 1.3%. The result suggests the formation of  $\text{PM} < 1 \mu\text{m}$  seldom derives from char fragmentation and included mineral coalescence, which is similar to actual pulverized coal combustion. With the increase in  $\varphi$ , the number of  $\text{PM}$ , especially  $1\text{--}10 \mu\text{m}$ , increases gradually. As mentioned previously, with the increase in  $\varphi$ , char fragmentation is more severe, whilst the probability of included minerals coalescence is reduced obviously; thus, more fine  $\text{PM}$  are formed, and the number of  $\text{PM} < 10 \mu\text{m}$  obviously enhances, which is an agreement with the previous results [16,22].

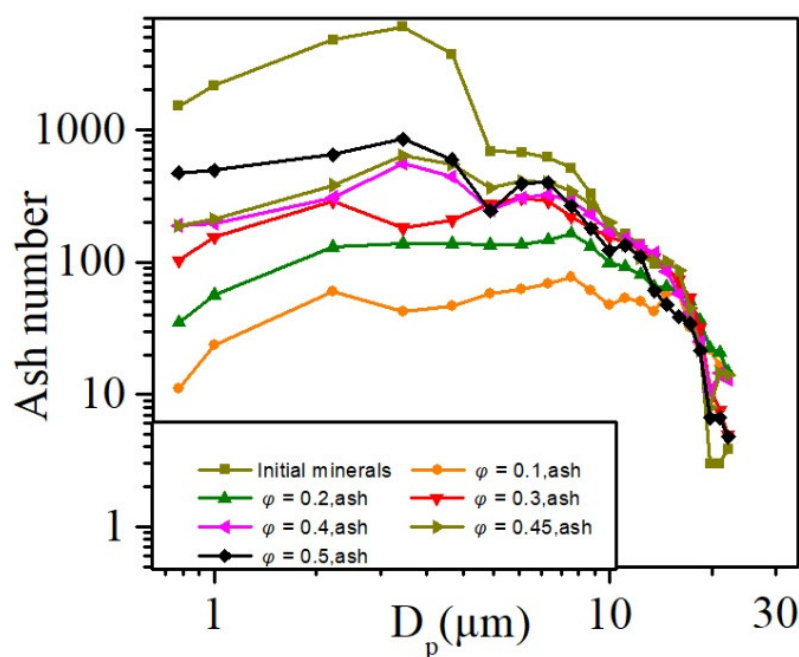


Figure 10. Particle number size distribution.

The particle volumetric size distribution from different initial porosity is shown in Figure 11; based on the hypothesis that all particles have the same density, particle volume size distribution can represent particle concentration size distribution approximately. Similarly with the number, since the frequency of fragmentation events increases with the increasing porosity, the average size of final ash particles is smaller for chars with higher macro-porosity, so that the concentration of PM, especially 1–10  $\mu\text{m}$ , increases gradually. In the condition of  $\varphi \geq 0.4$ , the concentrations of PM < 10  $\mu\text{m}$  are high, and their curves of size distribution are similar, which is attributed to porous char in the range of  $\varphi \geq 0.4$ , which leads to the phenomena of fragmentation, are all universal during char combustion and the concentrations from different  $\varphi$  have little difference. From the figure, the coarse mode peaks are distributed mainly at 12–13  $\mu\text{m}$ , while the other lower peak can be found at  $\sim 10 \mu\text{m}$  for  $\varphi = 0.45$  and 0.5. The advancement of peak value is attributed to more pores which cause more severe break up, and another finer PM peak is formed. A small peak located at 3  $\mu\text{m}$  can be found by the combustion of char of  $\varphi = 0.5$ , implying the observation of central mode caused by the relative porous char combustion. This distribution predicted by simulation is similar to those peak ranges of the central mode and the super-micron mode observed experimentally [16,22]. More experimental data are needed to validate and improve the ash formation model in future work.

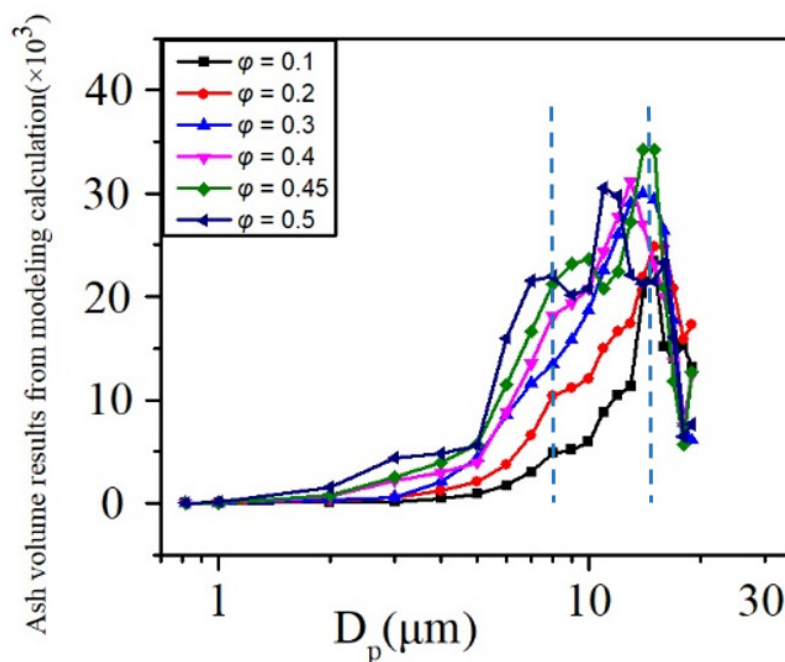


Figure 11. Particle volumetric (concentration) size distribution.

#### 4. Conclusions

A site percolation model of char fragmentation and mineral partitioning during dense and porous char combustion in a kinetically controlled regime is reported in this paper. Following conclusions can be drawn: increasing porosity enhances the surface reaction area and the number of fragments. The number of fragments and surface reaction area is higher for  $\varphi \geq 0.4$  compared to that for  $\varphi < 0.4$ . The char fragmentation concentrates on the early stage of char conversion gradually with increasing  $\varphi$ ; if  $\varphi \geq 0.4$ , char fragmentation obviously focuses on the conversion stage of 0.4–0.6, and the tendency with peak value transferring to the earlier conversion stage can be found. With the increase in  $\varphi$ , the number of PM, especially 1.0–10  $\mu\text{m}$ , increases gradually, as does concentration. In the condition of  $\varphi \geq 0.4$ , the concentrations of PM < 10  $\mu\text{m}$  are high, and their size of curves distribution are relatively similar. The coarse mode peaks are distributed mainly at 12–13  $\mu\text{m}$ , and a small peak located at 3  $\mu\text{m}$  can be found by the combustion of char of  $\varphi = 0.5$ . It is similar to those peak ranges of the central mode, and super-micron mode observed experimentally.

**Author Contributions:** Conceptualization, R.L.; methodology, R.L., C.W. and Z.J.; formal analysis, R.L., J.M. and Z.J.; investigation, R.L. and K.Y.; data curation, L.Q.; writing—original draft preparation, R.L., Z.J. and J.M.; writing—review and editing, J.M., L.Q. and C.W.; visualization, K.Y.; supervision, C.W.; project administration, C.W.; funding acquisition, J.M. and C.W. All authors have read and agreed to the published version of the manuscript.

**Funding:** This research was funded by the National Natural Science Foundation of China (Grant nos. 52076091) and the Open Project of State Key Laboratory of High-Efficiency Utilization of Coal and Green Chemical Engineering (No. 2021-K07).

**Institutional Review Board Statement:** Not applicable.

**Informed Consent Statement:** Not applicable.

**Data Availability Statement:** The data reported in this study will be available on request from the corresponding author.

**Conflicts of Interest:** The authors declare no conflict of interest.

## References

1. Xu, M.; Qiao, Y.; Zheng, C.; Li, L.; Liu, J. Modeling of homogeneous mercury speciation using detailed chemical kinetics. *Combust. Flame* **2003**, *132*, 208–218. [[CrossRef](#)]
2. Sheng, C.; Li, Y.; Liu, X.; Yao, H.; Xu, M. Ash particle formation during O<sub>2</sub>/CO<sub>2</sub> combustion of pulverized coals. *Fuel Process. Technol.* **2007**, *88*, 1021–1028. [[CrossRef](#)]
3. Luo, G.; Yao, H.; Xu, M.; Gupta, R.; Xu, Z. Identifying modes of occurrence of mercury in coal by temperature programmed pyrolysis. *Proc. Combust. Inst.* **2011**, *33*, 2763–2769. [[CrossRef](#)]
4. Zhu, Y.; Chen, Y.; Cheng, W.; Zhang, W.; Hu, J.; Zeng, K.; Yang, H.; Shao, J.; Chen, H. Reduction of fine particulate matter emissions from cornstalk combustion by calcium phosphates additives. *Fuel* **2021**, *283*, 119303. [[CrossRef](#)]
5. Sarofim, A.F.; Howard, J.B.; Padia, A.S. The physical transformation of the mineral matter in pulverized coal under simulated combustion conditions. *Combust. Sci. Technol.* **1977**, *16*, 187–204. [[CrossRef](#)]
6. Flagan, R.C.; Friedlander, S.K. *Recent Developments in Aerosol Science*; Shaw, D.T., Ed.; John Wiley & Sons: Hoboken, NJ, USA, 1978; pp. 25–59.
7. Linak, W.P.; Miller, C.A.; Seames, W.S.; Wendt, J.O.; Ishinomori, T.; Endo, Y.; Miyamae, S. On trimodal particle size distributions in fly ash from pulverized-coal combustion. *Proc. Combust. Inst.* **2002**, *29*, 441–447. [[CrossRef](#)]
8. Seames, W.S. An initial study of the fine fragmentation fly ash particle mode generated during pulverized coal combustion. *Fuel Process. Technol.* **2003**, *81*, 109–125. [[CrossRef](#)]
9. Yu, D.; Xu, M.; Yao, H.; Sui, J.; Liu, X.; Yu, Y.; Cao, Q. Use of elemental size distributions in identifying particle formation modes. *Proc. Combust. Inst.* **2007**, *31*, 1921–1928. [[CrossRef](#)]
10. Yu, D.; Xu, M.; Yao, H.; Liu, X.; Zhou, K. A new method for identifying the modes of particulate matter from pulverized coal combustion. *Powder Technol.* **2008**, *183*, 105–114. [[CrossRef](#)]
11. Liu, S.; Zhu, G.; Niu, Y.; Wen, L.; Lei, Y.; Wang, D. Characteristics of particulate emissions from coal char combustion: Char fragmentation and ash coalescence behaviors. *Fuel* **2022**, *310*, 122283. [[CrossRef](#)]
12. Gao, Q.; Li, S.; Zhao, Y.; Yao, Q. Mechanism on the contribution of coal/char fragmentation to fly ash formation during pulverized coal combustion. *Proc. Combust. Inst.* **2019**, *37*, 2831–2839. [[CrossRef](#)]
13. Mitchell, R.E.; Akanetuk, A.J. The impact of fragmentation on char conversion during pulverized coal combustion. *Symp. Combust.* **1996**, *26*, 3137–3144. [[CrossRef](#)]
14. Feng, B.; Bhatia, S.K. Percolative fragmentation of char particles during gasification. *Energy Fuels* **2000**, *14*, 297–307. [[CrossRef](#)]
15. Miccio, F. Modeling percolative fragmentation during conversion of entrained char particles. *Korean J. Chem. Eng.* **2004**, *21*, 404–411. [[CrossRef](#)]
16. Helble, J.J.; Sarofim, A.F. Influence of char fragmentation on ash particle size distributions. *Combust. Flame* **1989**, *76*, 183–196. [[CrossRef](#)]
17. Baxter, L.L. Char fragmentation and fly ash formation during pulverized-coal combustion. *Combust. Flame* **1992**, *90*, 174–184. [[CrossRef](#)]
18. Liu, G.; Wu, H.; Gupta, R.P.; Lucas, J.A.; Tate, A.G.; Wall, T.F. Modeling the fragmentation of non-uniform porous char particles during pulverized coal combustion. *Fuel* **2000**, *79*, 627–633. [[CrossRef](#)]
19. Kang, S.G.; Sarofim, A.F.; Beér, J.M. Effect of char structure on residual ash beér during pulverized coal combustion. *Symp. (Int.) Combust.* **1992**, *24*, 1153–1159. [[CrossRef](#)]
20. Salatino, P.; Miccio, F.; Massimilla, L. Combustion and percolative fragmentation of carbons. *Combust. Flame* **1993**, *95*, 342–350. [[CrossRef](#)]
21. Liu, X.; Xu, M.; Yao, H.; Yu, D.; Gao, X.; Cao, Q.; Cai, Y. Effect of combustion parameters on the emission and chemical composition of particulate matter during coal combustion. *Energy Fuels* **2007**, *21*, 157–162. [[CrossRef](#)]

22. Kang, S.G.; Kerstein, A.R.; Helble, J.J.; Sarofim, A.F. Simulation of residual ash formation during pulverized coal combustion: Bimodal ash particle size distribution. *Aerosol Sci. Technol.* **1990**, *13*, 401–412. [[CrossRef](#)]
23. Yu, D.; Xu, M. A Computer simulation study of char fragmentation. *Proc. CSEE* **2005**, *25*, 90–93. (In Chinese)
24. Yu, D.; Xu, M.; Huang, J.; Li, G.; Liu, X.; Yun, Y. A model study on char fragmentation and ash formation. *J. Eng. Thermophys.* **2005**, *26*, 1041–1044. (In Chinese)
25. Yu, D.; Xu, M.; Zhang, L.; Yao, H.; Wang, Q.; Ninomiya, Y. Computer-controlled scanning electron microscopy (CCSEM) investigation on the heterogeneous nature of mineral matter in six typical Chinese coals. *Energy Fuels* **2007**, *21*, 468–476. [[CrossRef](#)]
26. Tang, L.G.; Gupta, R.P.; Sheng, C.D.; Wall, T.F. A mechanistic approach to characterize coal heterogeneity in predicting high-temperature volatile matter yields. *Energy Fuels* **2004**, *18*, 1716–1722. [[CrossRef](#)]
27. Wang, H.; Li, H.; Chen, Q.; Gao, J.; Wang, C. Modified three-dimensional percolation simulation of char fragmentation and particulate formation. *AIP Adv.* **2017**, *7*, 025016. [[CrossRef](#)]
28. Quann, R.J. Ash Vaporization under Simulated Pulverized Coal Combustion Conditions. Ph.D. Thesis, Massachusetts Institute of Technology, Cambridge, MA, USA, 1982.
29. Gupta, R.P.; Wall, T.F.; Kajigaya, I.; Miyamae, S.; Tsumita, Y. Computer-controlled scanning electron microscopy of minerals in coal—implications for ash deposition. *Prog. Energy Combust. Sci.* **1998**, *24*, 523–543. [[CrossRef](#)]
30. Wen, C.; Gao, X.; Xu, M. A CCSEM study on the transformation of included and excluded minerals during coal devolatilization and char combustion. *Fuel* **2016**, *172*, 96–104. [[CrossRef](#)]
31. Wen, C.; Xu, M.; Zhou, K.; Yu, D.; Zhan, Z.; Mo, X. The melting potential of various ash components generated from coal combustion: Indicated by the circularity of individual particles using CCSEM technology. *Fuel Process. Technol.* **2015**, *133*, 128–136. [[CrossRef](#)]
32. Benfell, K.E.; Liu, G.S.; Roberts, D.G.; Harris, D.J.; Lucas, J.A.; Bailey, J.G.; Wall, T.F. Modeling char combustion: The influence of parent coal petrography and pyrolysis pressure on the structure and intrinsic reactivity of its char. *Proc. Combust. Inst.* **2000**, *28*, 2233–2241. [[CrossRef](#)]
33. Edwards, D.A.; Hanes, J.; Caponetti, G.; Hrkach, J.; Ben-Jebria, A.; Eskew, M.L.; Mintzes, J.; Deaver, D.; Lotan, N.; Langer, R. Large porous particles for pulmonary drug delivery. *Science* **1997**, *276*, 1868–1872. [[CrossRef](#)]
34. Wen, C.; Gao, X.; Yu, Y.; Wu, J.; Xu, M.; Wu, H. Emission of inorganic PM<sub>10</sub> from included mineral matter during the combustion of pulverized coals of various ranks. *Fuel* **2015**, *140*, 526–530. [[CrossRef](#)]